American Mineralogist, Volume 83, pages 1426–1443, 1998

Bacterial reduction of crystalline Fe^{3+} oxides in single phase suspensions and subsurface materials

JOHN M. ZACHARA,* JAMES K. FREDRICKSON, SHU-MEI LI, DAVID W. KENNEDY, STEVEN C. SMITH, AND PAUL L. GASSMAN

Pacific Northwest National Laboratory, Richland, Washington 99352, U.S.A.

ABSTRACT

Microbiologic reduction of synthetic and geologic Fe^{3+} oxides associated with four Pleistocene-age, Atlantic coastal plain sediments was investigated using a dissimilatory Fe reducing bacterium (*Shewanella putrefaciens*, strain CN32) in bicarbonate buffer. Experiments investigated whether phosphate and anthraquinone-2, 6-disulfonate, (AQDS, a humic acid analogue) influenced the extent of crystalline Fe^{3+} oxide bioreduction and whether crystalline Fe^{3+} oxides in geologic materials are more or less reducible than comparable synthetic phases. Anaerobic incubations (10^8 organisms/mL) were performed both with and without PO_4 and AQDS that functions as an electron repository and shuttle. The production of Fe^{2+} (solid and aqueous) was followed with time, as was mineralogy by X-ray diffraction. The synthetic oxides were reduced in a qualitative trend consistent with their surface area and free energy: hydrous ferric oxide (HFO)>goethite>hematite. Bacterial reduction of the crystalline oxides was incomplete in spite of excess electron donor. Biogenic formation of vivianite [$Fe_3(PO_4)_2 \cdot 8H_2O$] and siderite ($FeCO_3$) was observed; the conditions of their formation was consistent with their solubility. The geologic Fe^{3+} oxides showed a large range in reducibility, approaching 100% in some materials. The natural oxides were equally or more reducible than their synthetic counterparts, in spite of association with non-reducible mineral phases (e.g., kaolinite). The reducibility of the synthetic and geologic oxides was weakly effected by PO_4, but was accelerated by AQDS. CN32 produced the hydroquinone form of AQDS (AHDS), that, in turn, had thermodynamic power to reduce the Fe^{3+} oxides. As a chemical reductant, it could reach physical regions of the oxide not accessible by the organism. Electron microscopy showed that crystallite size was not the primary factor that caused differences in reducibility between natural and synthetic crystalline Fe^{3+} oxide phases. Crystalline disorder and microheterogeneities may be more important.

INTRODUCTION

Dissimilatory metal reducing bacteria (DMRB) are an important group of microorganisms that reduce metal oxides in geochemical environments. Under anoxic conditions, these organisms can use Fe^{3+} [or Mn^{4+}] as electron acceptors coupled to the oxidation of organic matter or H_2, and gain energy for maintenance and growth from such reactions. Fe^{3+} and Mn^{4+} reduction is directly (enzymatically) linked to the electron transfer chain in DMRB (Myers and Myers 1997). DMRB are common in groundwaters and sediments (Coates et al. 1995; Fredrickson and Gorby 1996) and influence the aqueous geochemistry, surface chemistry, and mineralogy of these environments (Baedecker et al. 1992; Chapelle 1993; Lovley et al. 1990; Chapelle and Lovley 1992). DMRB also influence the Fe^{2+} mineralization of geologic materials and sediments. The formation of siderite, magnetite, and vivianite are generally attributed to the activity of DMRB (Mortimer et al. 1997; Postma 1981; Pye et al. 1990; Suess 1979) but little is known about the role of the microorganisms in such mineralization and if their contribution is direct or indirect.

Fe^{3+} and Mn^{4+} oxides are insoluble at the pH of most natural waters and so differ from soluble, aqueous electron acceptors such as O_2 and NO_3 that are also used by facultative DMRB. As a result of low solubility, direct contact between the DMRB and the oxide surface is required for reduction to occur (Arnold et al. 1988; Lovley et al. 1991; Myers and Nealson 1988). Whereas the total aqueous concentration of a dissolved electron acceptor may be utilized by a microorganism, more complex, but unresolved relationships exist when the electron acceptor is associated with a solid phase. Preliminary studies indicated that amorphic or poorly crystalline oxides were the bioavailable Fe^{3+} form in aquatic sediments (Lovley and Phillips 1987; Phillips et al. 1993). It is now clear, however, that amorphous, poorly crystalline, and crystalline Fe^{3+} oxides are all available, to varying degrees, for

* E-mail: jm_zachara@ppnl.gov.

0003–004X/98/1112–1426$05.00

reduction by DMRB (Arnold et al. 1988; Phillips et al. 1993; Roden and Zachara 1996). Many factors appear to control the extent of Fe^{3+} oxide reduction in presence of excess electron donor, including: medium composition; post-reduction geochemical reactions; the structural, thermodynamic, and surface chemical properties of the solid-phase oxide; and physiological factors related to DMRB metabolic status and growth stage. The interrelationships between these factors and their quantitative effects have not been established.

Recently we investigated the bacterial reduction (by *Shewanella putrefaciens*) of amorphous hydrous ferric oxide (HFO) in different buffers both without and with a quinone (anthraquinone-2, 6-disulfonate, AQDS) that functions as an electron shuttle (Fredrickson et al. 1998). The AQDS enhances microbial respiration and electron delivery to the oxide, and contains a quinone group that is known to be present in humic substances (Stevenson 1985; Thorn et al. 1992). The DMRB transformed the HFO into magnetite, siderite, vivianite, and/or green rust (Fredrickson et al. 1998). The identity of the secondary phases formed and their crystallinity were influenced by the buffer composition, the presence of P, and the respiration/reduction rate that was enhanced by AQDS. The nature of mineralization accompanying reduction was found to influence the extent of Fe^{3+} reduction.

Magnetite formation, for example, was found to sequestor 60% of the Fe^{3+} in a form that was not available to *S. putrefaciens* under the experimental conditions examined. AQDS was found to increase the bioreduction rate of HFO, but the HFO was fully transformed to secondary mineral products regardless of whether AQDS was present or not. It is not known whether comparable minerals result from the bioreduction of crystalline Fe^{3+} oxides, or whether humic acid analogues such as AQDS can enhance the extent of bioreduction of crystalline Fe^{3+} oxides, which unlike HFO, are generally not fully reduced by DMRB (Roden and Zachara 1996).

Here we investigate chemical and mineralogic factors influencing the bacterial reducibility of synthetic and natural Fe^{3+} oxides. Our objectives were: (1) to define the effects of an electron shuttle (AQDS) and nutrient phosphate (via vivianite precipitation) on the extent of bacterial reduction of crystalline Fe^{3+} oxides (e.g., percent Fe^{3+} reduced) and, (2) to determine if crystalline Fe^{3+} oxides of geologic origin were more, less, or equally reducible than synthetic solids and the causes for differences if observed. The experimental system involved synthetic HFO, goethite, and hematite, and four sandy-textured, Pleistocene-age, poorly consolidated subsurface sediments containing grain coatings or surface precipitates of crystalline Fe^{3+} oxides. These solid phases were inoculated with a facultative subsurface DMRB (*S. putrefaciens*, CN32) in bicarbonate buffer, both with and without AQDS and PO_4, using lactate as the electron donor. The evolution of chemical [Fe^{2+}, acetate] and mineralogic byproducts and the DMRB population were followed with time as a basis for defining mineralogic controls on respiration and bioreduction.

Experimental procedures

Fe^{3+} oxides and sediments

Hydrous ferric oxide (HFO) was prepared by neutralization of a $FeCl_3 \cdot 6H_2O$ solution with NaOH followed by repeated washing with deionized water to remove chloride (Lovley and Phillips 1986). A medium surface area goethite (52.3 m^2/g) and hematite (5.2 m^2/g) were prepared by hydrolysis of Fe^{3+} solutions and aging at elevated temperatures according to procedures of Schwertmann and Cornell (1991). The precipitates were extracted three times with acidified hydroxyl-amine hydrochloride (Chao and Zhou 1983) to remove potentially residual ferrihydrite, washed repeatedly to remove residual extractants, dialyzed against deionized distilled H_2O, freeze-dried, and stored in a glovebox under anaerobic conditions. Freeze drying was used to stabilize the solid phases as stored aqueous suspensions often develop biofilms. Both goethite and hematite were well crystallized, displayed characteristic *d*-values consistent with literature values, and were free of crystallographic impurities at the level discernible by X-ray diffraction (XRD).

Unconsolidated, sandy-textured geologic materials were collected from Pleistocene-age, Atlantic Coastal Plain sediments in Oyster, VA, Milford DE, and Eatontown, NJ. The sampling depths were approximately 3 m below land surface; overriding surface soils were characterized as Ultisols. The sediments are beach deposits and are dominated by sand textured quartz grains. Crystalline Fe^{3+} oxides exist as grain coatings, discrete microprecipitates, and intergrain cements in these sediments imparting a yellowish-orange to red coloration to the sediment. Kaolinite and poorly crystalline Al-oxides exist as primary, fine-grained (<2.0 μm) accessory phases to the Fe^{3+} oxides. The mineralogy of two of these locations (Oyster and Milford) was reported (Zachara et al. 1995).

The subsurface sediments were air-dried and passed through a 2 mm sieve prior to characterization or use. Surface area was measured by multipoint $N_{2(g)}$ adsorption with B.E.T analysis. Extractable oxides were determined using three techniques: hydroxylamine hydrochloride was used for the extraction of amorphous Fe oxyhydroxides and reducible manganese oxides (Chao and Zhou 1983), dithionite-citrate-bicarbonate (DCB) was used for extraction of reducible Fe oxides (Mehra and Jackson 1960), and ammonium oxalate was used for removal of amorphous aluminosilicates as well as poorly crystalline Fe oxides (Schwertmann 1964; Fey and LeRoux 1977).

The medium used in all experiments contained trace minerals (Table 1). Nitrilotriacetic acid (NTA), a complexing agent, was included as common practice to maintain solubility of the cationic metals at circumneutral pH. The stability constants for the dominant NTA complexes of the trace metals (from Smith and Martell 1997) are shown in Table 1. NTA has potential to influence bacte-

TABLE 1. Medium composition

Components	Concentration, *M*	log K_{NTA}*
Na lactate	2.7×10^{-2}	
NH_4Cl	2.5×10^{-2}	
KCl	1.2×10^{-3}	
$CaCl_2$	6.1×10^{-4}	7.67 ($CaNTA^-$)
Nitrilotriacetic acid	7.1×10^{-4}	
$MgSO_4 \cdot 7H_2O$	1.1×10^{-3}	6.75 ($MgNTA^-$)
NaCl	1.5×10^{-3}	
$MnSO_4 \cdot H_2O$	2.7×10^{-4}	9.5 ($MnNTA^-$)†
$ZnCl_2$	8.6×10^{-5}	11.9 ($ZnNTA^-$)
$FeSO_4 \cdot 7H_2O$	3.2×10^{-5}	9.85 ($FeNTA^-$)
$CaCl_2 \cdot 2H_2O$	6.1×10^{-5}	
$CoCl_2 \cdot 6H_2O$	3.8×10^{-5}	11.7 ($CoNTA^-$)
$Na_2MoO_4 \cdot 2H_2O$	9.3×10^{-6}	
$Na_2WO_4 \cdot 2H_2O$	6.8×10^{-6}	
$NiCl_2 \cdot 6H_2O$	9.1×10^{-6}	12.8 ($NiNTA^-$)
$CuSO_4 \cdot 5H_2O$	3.6×10^{-6}	13.1 ($CoNTA^-$)
$AlK(SO_4)_2 \cdot 12H_2O$	1.9×10^{-6}	
H_3BO_3	1.5×10^{-5}	
$NaHCO_3$	3.0×10^{-2}	
NaH_2PO_4‡	3.9×10^{-3}	
anthraquinone-2, 6-disulfonate‡	9.0×10^{-5}	

* I = 0, T = 25 °C (I = ionic strength).
† Estimated.
‡ Treatment-specific components.

rial Fe reduction by solubilizing both Fe^{3+} (Lovley and Woodward 1996) and biogenic Fe^{2+} (Urrutia et al., unpublished manuscript). Experiments and speciation calculations by our group (Zachara et al., unpublished manuscript) and others (Urrutia et al., unpublished manuscript) have shown that the trace metals and NTA (at 0.7 m*M)* have little or slight discernable impact on the extent of bacterial Fe^{3+} oxide reduction under conditions identical to those used in this study. The NTA, under these conditions, is saturated to large degree by cations with either a larger stability constant (e.g., Cu, Ni, Zn, and Co; Table 1) or in higher concentration (e.g., Ca/Mg) than Fe^{2+}. NTA enhances the extent of bacterial reduction of crystalline Fe^{3+} oxides at concentrations in excess of 1m*M* (Urrutia et al., unpublished manuscript) because of aqueous complexation and other reasons that have not been fully resolved. The chemical behavior of NTA-metal complexes in oxide suspensions is complex and not easily generalized (Girvin et al. 1996).

Bacteria and media

S. putrefaciens strain CN32 (Subsurface Microbial Culture Collection) was provided courtesy of Dr. David Boone (Oregon Graduate Institute). Strain CN32 was isolated from a subsurface core sample (250 m beneath the surface) obtained from the Morrison Formation during drilling of a shale-sandstone sequence in northwestern New Mexico. The sediments were anaerobic at the time of collection based on appearance (blue-green in color) and high Fe^{2+} content, >1.5 g of 0.5 N HCl-extractable Fe^{2+}/kg. Also, groundwater sampled from the overlying Cubero Sandstone had DO below detections (<0.2 mg/L) and Fe^{2+} and S^{2-} concentrations at 0.8 and 13.6 mg/L, respectively (Fredrickson et al. 1997). The organism was identified as *S. putrefaciens* by phylogenetic analysis of the 16S rRNA gene sequence (D. Boone, unpublished results). CN32 was routinely cultured aerobically in tryptic soy broth (TSB), 30 g/L (Difco Laboratories, Detroit, Michigan) and stock cultures were maintained at −80 °C.

The components in the defined medium used for the Fe reduction experiments are listed in Table 1. The medium was buffered with 30 m*M* $NaHCO_3$. Sodium lactate (20 m*M)* was added as the electron donor and, in select treatments, filter-sterilized (0.2 μm) anthraquinone-2, 6-disulfonate (AQDS, Sigma Chemical Co., St. Louis, Missouri) was added separately. Medium was dispensed into Balsch tubes, purged with O_2-free N_2:CO_2 (80:20), stopped with butyl rubber closures, crimp sealed, and autoclaved.

CN32 cells were harvested by centrifugation from TSB cultures, washed with buffer to remove residual TSB, resuspended in bicarbonate and purged with O_2-free N_2. Cells were added to media to obtain a final concentration of 2.4×10^8 cells/mL. HFO was maintained as an aqueous suspension under anaerobic conditions and was added to media to obtain a final concentration of 50 m*M*. The crystalline Fe^{3+} oxides were added as lyophilized powders under anaerobic conditions to a total Fe^{3+} concentration of 50 m*M*. Air dry sediments were added at a mass concentration to yield 1 g of <2.0 mm sediment per 10 mL of media. Unlike the Fe^{3+} oxide suspensions, the total reducible Fe^{3+} concentrations in the sediment incubations was variable, but in all cases electron donor (lactate) was present in excess of that required to microbially reduce all of the Fe^{3+} present. Tubes were incubated in the dark at 30 °C and agitated at 100 rpm. Each treatment was replicated three times and separate tubes were sacrificed at each time-point for analyses. Controls consisted of media that received 1 mL of sterile, anaerobic buffer in place of CN32 cell suspension.

Fe^{2+} production in DMRB (TSB grown) inoculated, Fe^{3+} oxide suspensions with excess e-donor follows an approximate linear rate during the early stages of reduction (Roden and Zachara 1996; Urrutia et al. 1998; Fredrickson et al. 1998). After this linear phase, reduction slows and eventually ceases after periods ranging from less than 20 to over 50 days depending on oxide, buffer, and inoculum. The rate reduction results from depletion of the electron acceptor [e.g., Fe^{3+}], chemical and mineralogic change to the aqueous and solid phase, thermodynamic barriers, enzyme deactivation, cell mortality, and other complex and unresolved chemical and physiological factors. All inoculated suspensions of Fe^{3+} oxide and subsurface sediments were incubated slightly beyond the time point where the biotic reduction reaction ceased. This period ranged from 27–40 d and is considered one cell cycle.

Analyses

At select time-points, replicate tubes were removed from the incubator and transferred to an anaerobic (Ar:H_2, 95:5) glovebag (Coy Laboratory Products, Inc., Ann

Arbor, Michigan). Butyl rubber stoppers were removed and one mL of suspension was removed and filtered through a 0.2 μm polycarbonate filter directly into one mL of 0.5 N Ultrex HCl. This fraction was considered as the soluble fraction and analyzed for Fe^{2+}, phosphate, lactate, acetate, and reduced AQDS, where appropriate. The filtration step was shown to be effective in the removal of both fine-grained Fe^{3+} oxides and biogenic products (Fredrickson et al. 1998). In another aliquot, pH was measured under anaerobic conditions using a Ross combination electrode. HCl-extractable Fe^{2+} was obtained by placing 1 mL of suspension directly into one mL of 2N Ultrex HCl, mixing, and allowing equilibration for at least one hour before analyzing for Fe^{2+}. The 2N HCl extraction has been shown to be effective in the dissolution of most Fe^{2+} compounds resulting from bacterial Fe reduction, with the possible exception of coarse-grained crystalline magnetite (Fredrickson et al. 1998).

Fe^{2+} in acidified filtrates (0.2 μm) or extracts was determined using the ferrozine assay (Lovley and Phillips 1986). Phosphate concentrations were determined using an ammonium paramolybdate assay (Olsen and Sommers 1982). Lactate and acetate were determined at the final sampling time-points by HPLC. Reduced AQDS was quantified by measuring the absorbance of the reduced form, anthradihydroquinone-2, 6-disulfonate (AHDS), at 405 nm. Major cations (Ca, Na) were analyzed by ICP-AES and anions (Cl^-) by ion chromatography. Inorganic carbon was measured on an unacidified aliquot, and HCO_3 was computed from the final pH, ionic strength, and ionization constants.

X-ray diffraction

Mineral residue from the reduction experiments was mixed with glycerol under anaerobic conditions and the solid slurry was smeared on a glass slide for X-ray diffraction (XRD) analysis. The slides were maintained under anoxic atmosphere until the time of analysis. The XRD apparatus consisted of two Philips Wide-Range Vertical Goniometers with incident-beam 2θ compensating slits, soller slits, fixed 2 mm receiving slits, diffracted beam graphite monochromators, and scintillation counter detectors. The X-ray source was a Philips XRG3100 X-ray Generator operating a fixed-anode, long-fine-focus Cu tube at 45 Kv, 40 mA (1800 W). Instrument control was by means of Databox NIMBIM modules (Materials Data Inc., Livermore, California). The International Center for Diffraction Data Powder Diffraction File database on CD-ROM (ICDD PDF-2, Sets 1-46 1996) was the source of reference powder diffraction data.

Electron microscopy

Samples of synthetic goethite and hematite, and Fe^{3+} oxide-containing mineral separates of the Milford and Eatontown hematite sediments were examined using a field emission scanning electron microscope (FESEM) manufactured by LEO (model 982) to obtain crystal morphology and qualitative chemical compositions. Morphologic analyses were performed at 5 keV and 90 μA and utilized the below lens detector or in-lens detector, or a combination of the two. Compositional analyses by energy dispersive spectrometry (EDS) utilized a liquid nitrogen cooled Oxford Pentafet detector with the microscope operating at 20 keV accelerating potential and 90 μA current.

Thermodynamic calculations

Thermodynamic calculations were performed to assess the degree of solubility equilibrium of the biogenic precipitates, and to predict stable solid phase mineral assemblages as a function of pe, pH, buffer composition, and P concentration. These calculations were performed with the MINTEQA2 code (Allison et al. 1991) and a thermodynamic database assembled by the authors that contained the best available equilibrium constants for pertinent aqueous species and solid phases. Thermodynamic data for the Fe^{2+}-CO_3^{2-}-H_2O and the Fe^{2+}-PO_4^{3-}-H_2O systems were taken from Bruno, et al. (1992) and Al-Borno and Tomson (1994), respectively. Other thermodynamic data was taken from Smith and Martell (1997) and Wagman et al. (1982).

Results

Microbial reduction of single phase oxides

Reduction extent and Fe/P chemistry. The HCl extraction is effective in solubilizing most biogenic Fe^{2+} solid phases (Fredrickson et al. 1998), and it is used here as a measure of the total extent of reduction (i.e., Fe^{2+} production). All three single phase oxides (hematite, goethite, and HFO) were reduced to variable extents by *S. putrefaciens* in bicarbonate buffer with 4 m*M* PO_4, but the presence of 100 μ*M* AQDS stimulated reduction (Fig. 1a). The stimulatory effect was greatest after 4 days and was most substantial for hematite where the total extent of reduction (after 39 d) was increased by over ten-fold (Table 2). Almost all the HFO was reduced (95%) after 39 days, and the extent of goethite reduction was enhanced by a factor of 3.5 when AQDS was present (Table 2). In the absence of AQDS, <1% of the hematite was reduced and approximately 9% of the goethite was reduced. These values are in ratio to the surface area of the two crystalline oxides, and the extent of reduction without AQDS was consistent with that observed for these same oxides using a different *Shewanella* strain (*S. alga*, strain BrY; Roden and Zachara 1996).

Soluble Fe^{2+} increased with time and reduction extent for all three oxides in the absence of AQDS (Fig. 1b). Fe^{2+} is strongly sorbed by all three oxides at circumneutral pH (Fredrickson et al. 1998), and for that reason as well as precipitation (to be discussed below), aqueous Fe^{2+} concentrations were below those extracted by HCl. Phosphate acts to counteract Fe^{2+} sorption through formation of strong aqueous complexes. As will be shown below, however, P concentrations changed during the course of bioreduction. AQDS caused marked increases in aqueous Fe^{2+} concentration (Fig. 1b), with those for

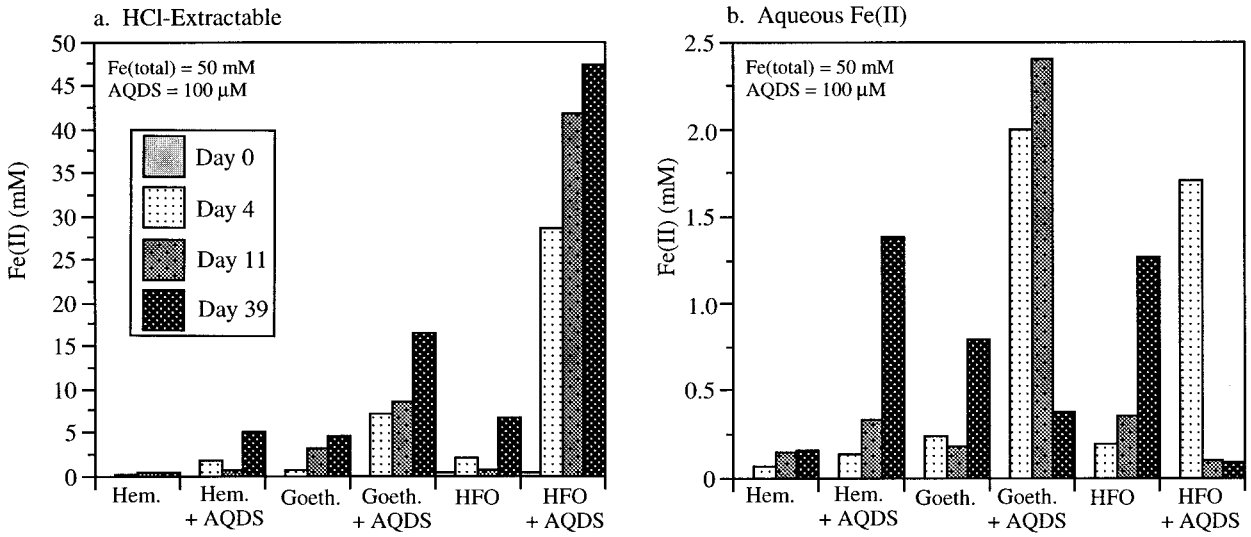

FIGURE 1. HCl-extractable (**a**) and aqueous Fe^{2+} (**b**) observed in bioreduction experiments with synthetic Fe^{3+} oxides, including goethite, hematite, and hydrous ferric oxide (HFO). Results show the impact of AQDS. All experiments contained bicarbonate buffer and 4 m*M* PO_4.

hematite and goethite being most dramatic (approximately ten-fold). $Fe^{2+}_{(aq)}$ concentrations decreased with time in the goethite and HFO suspensions with AQDS. Fe^{2+} precipitation in biogenic solids, surface roughening providing more sites for Fe^{2+} adsorption, or retarded Fe^{2+} detachment with reduction extent may explain this observed trend.

Phosphate, at 4 m*M* concentration, is a normal constituent of the basal media used to culture and to study DMRB/Fe^{3+} oxide reductive mechanisms (Kostka and Nealson 1995; Lovley and Phillips 1986; Lovley and Phillips 1988; Lovley et al. 1991; Mortimer and Coleman 1997; Roden and Zachara 1996). Phosphate is strongly sorbed by Fe oxides (Colombo et al. 1994; Geelhoed et al. 1997; Nilsson et al. 1992; Torrent et al. 1992) and has been shown to influence the nature of mineralization resulting from the bioreduction of HFO (Fredrickson et al. 1998). In the absence of CN32 cells, $PO_{4(aq)}$ concentrations showed the impact of increasing degrees of sorption through the series hematite<goethite<<HFO (Fig. 2a).

TABLE 2. Extent of reduction of synthetic single phase Fe^{3+} oxides

Oxide	Fe^{2+}-HCl (m*M*)	% Reduced
Hematite*	0.3	0.6
Hematite + AQDS*	5.0	9.9
Goethite	4.6	9.2
Goethite + AQDS	16.4	32.8
HFO	6.7	13.4
HFO + AQDS	47.3	94.6

Notes: Reduction by *S. putrefaciens* CN32 in suspension with 4 m*M* PO_4. The initial concentration of each oxide was 50 m*M* Fe^{3+} and the equilibration time was 39 days.
* Experiment 1, no X-ray diffraction collected.

HFO was highly effective at sorbing P. The extent of sorption noted on the three phases was consistent with their surface area and the anion-sorbing site concentrations of the different suspensions. The 4 m*M* PO_4 overwhelmed the sorption capacity of the two crystalline oxides, with a majority of the PO_4 remaining as a soluble constituent in the absence of DMRB metabolism.

Aqueous PO_4 varied greatly with time in some of the oxide suspensions inoculated with CN32 (Fig. 2b). In suspensions with the crystalline oxides, $PO_{4(aq)}$ concentrations decreased as Fe^{2+} was generated by bioreduction. There was close parallel between the concentration of HCl-extractable Fe^{2+} and decrease in $PO_{4(aq)}$ that was most evident for goethite and hematite with AQDS. AQDS, which enhanced oxide bioreduction, also stimulated PO_4 loss from solution in the crystalline oxide suspensions. This effect was most pronounced for hematite, where phosphate concentrations remained high during the course of incubation without AQDS, but decreased fourfold with AQDS. Aqueous PO_4 concentrations in the HFO suspension were further depressed over those noted in the abiotic controls, but time variant effects and correlations with the extent of reduction were not evident. The decrease in $PO_{4(aq)}$ may be attributed to assimilation by bacterial cells, or to precipitation reactions with Fe^{2+}.

Mineralogic transformations. The synthetic goethite and hematite were compositionally pure, highly crystalline, and exhibited typical morphologies associated with such laboratory preparations. The goethite existed as approximate 500 nm laths and the hematite as 300 nm spheres (Fig. 3). Both were present as 2–10 µm aggregates in the freeze-dried powders used as material sources for the bioreduction experiments. Electron microscopy of suspensions showed that these aggregates dispersed to

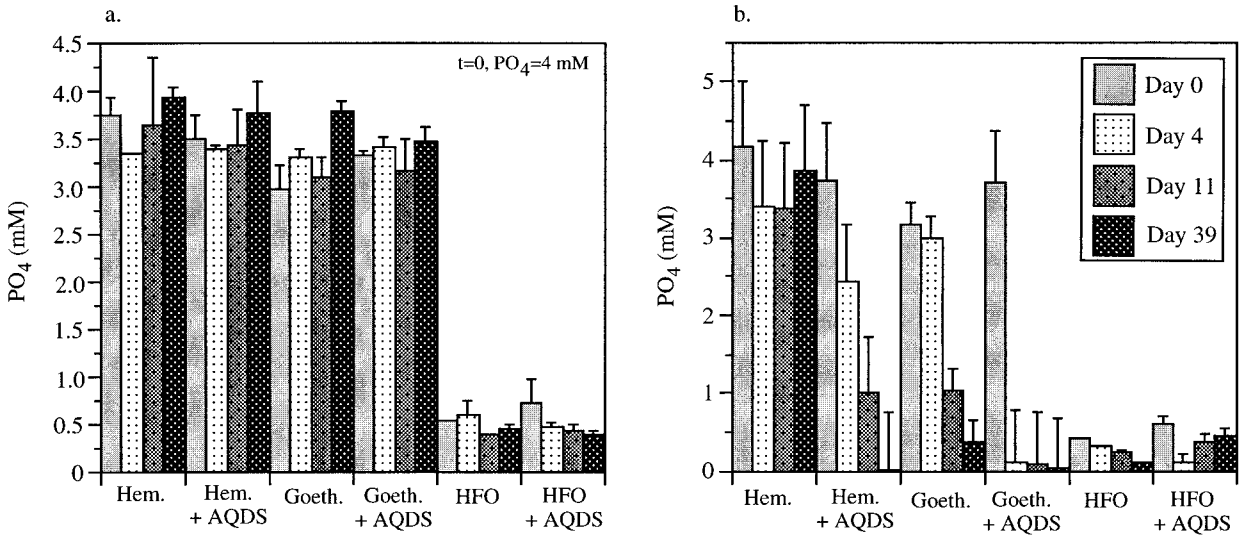

FIGURE 2. Soluble PO_4 in Fe^{3+} oxide suspensions without (**a**) and with (**b**) CN32 inoculum.

smaller flocs (≈1–2 μm) containing 5–10 crystallites when placed in the incubation media (not shown).

Mineralogic changes to many of the Fe^{3+} oxides accompanied bioreduction. Fredrickson et al. (1998) showed that HFO was fully transformed by CN32 to a mixture of siderite and vivianite after 7 d in bicarbonate buffer with 4 m*M* P. Mineral products were the same both with and without AQDS, but AQDS enhanced the apparent crystallinity of carbonate and phosphate solids as evidenced by sharper XRD peaks with higher count rates. In the bioreduction experiments here, the crystalline Fe^{3+} oxides were only partially reduced (e.g., 2–30%), but crystalline products were nonetheless observable by XRD.

Vivianite was observed in goethite suspension after 11 d in presence of AQDS and P (Fig. 4), and a combination of both vivianite and siderite was identified after 39 d (Fig. 4). Vivianite, therefore, formed before siderite as a bioreduction product in presence of 4 m*M* P. Both vivianite and siderite were removed by the HCl extraction (Fig. 4). The signal-to-noise ratio of the goethite diffraction pattern was improved after HCl extraction, possibly by removal of other amorphous or poorly crystalline ferrous products. In the absence of P with AQDS, siderite was the only crystalline reduction product of goethite observed by XRD in bicarbonate buffer when approximately 25% of the solid was reduced (Fig. 4). In the absence of AQDS, lessor amounts of goethite were reduced by CN32 (approximately 15%). Under these conditions, vivianite was the only reduction product when P was present and no crystalline products were observed by XRD in its absence (not shown). Crystalline reduction products were only observable for hematite in the presence of AQDS and P, where vivianite was observed (Fig. 5). Magnetite, a biogenic transformation product of HFO (Fredrickson et al. 1998) was not observed by XRD in any of crystalline Fe^{3+} oxide incubations.

Microbial reduction of subsurface materials

Bioreduction extent and Fe/P chemistry. *S. putrefaciens* was effective in utilizing Fe^{3+} oxides in the subsurface materials as an electron acceptor. Millimolar concentrations of Fe^{2+} were generated by CN32 in bicarbonate buffer (Fig. 6a). The amount of Fe^{2+} produced was in qualitative proportion to the mass of Fe^{3+} removed by dithionite-citrate-bicarbonate (DCB) extraction of the sediments (Table 3). The highest concentration of evolved Fe^{2+} was observed in the Eatontown hematite sediment that had the highest concentration of DCB extractable Fe^{3+} (366 μmol/g). A direct relation between Fe^{3+} reduction with the amount of poorly crystalline components, as extracted by $NH_2OH{\cdot}HCl$ or ammonium oxalate, was not evident. Phosphate is a required nutrient for growth, but the bioreduction of Fe^{3+} oxides in the subsurface materials was not sensitive to its presence or absence. To a large degree, equivalent amounts of Fe^{3+} reduction were observed in suspensions of similar composition with and without PO_4 (Fig. 6a, Table 4).

Unlike the effect of PO_4, however, AQDS had a clear stimulatory effect on reduction of the natural Fe^{3+} oxides, increasing their availability as electron acceptors for respiring microorganisms (Fig. 6a; Table 4). This stimulatory effect was similar to, but less pronounced, than observed for the synthetic oxides. AQDS increased the extent of bioreduction of the synthetic solids at experiment termination by factors of 3.5 to over 10 (Table 2), whereas the enhancement noted for the subsurface materials ranged from 1.2 to 2.2. The effect of AQDS was reduced by PO_4 in all the subsurface sediments except the Eatontown hematite.

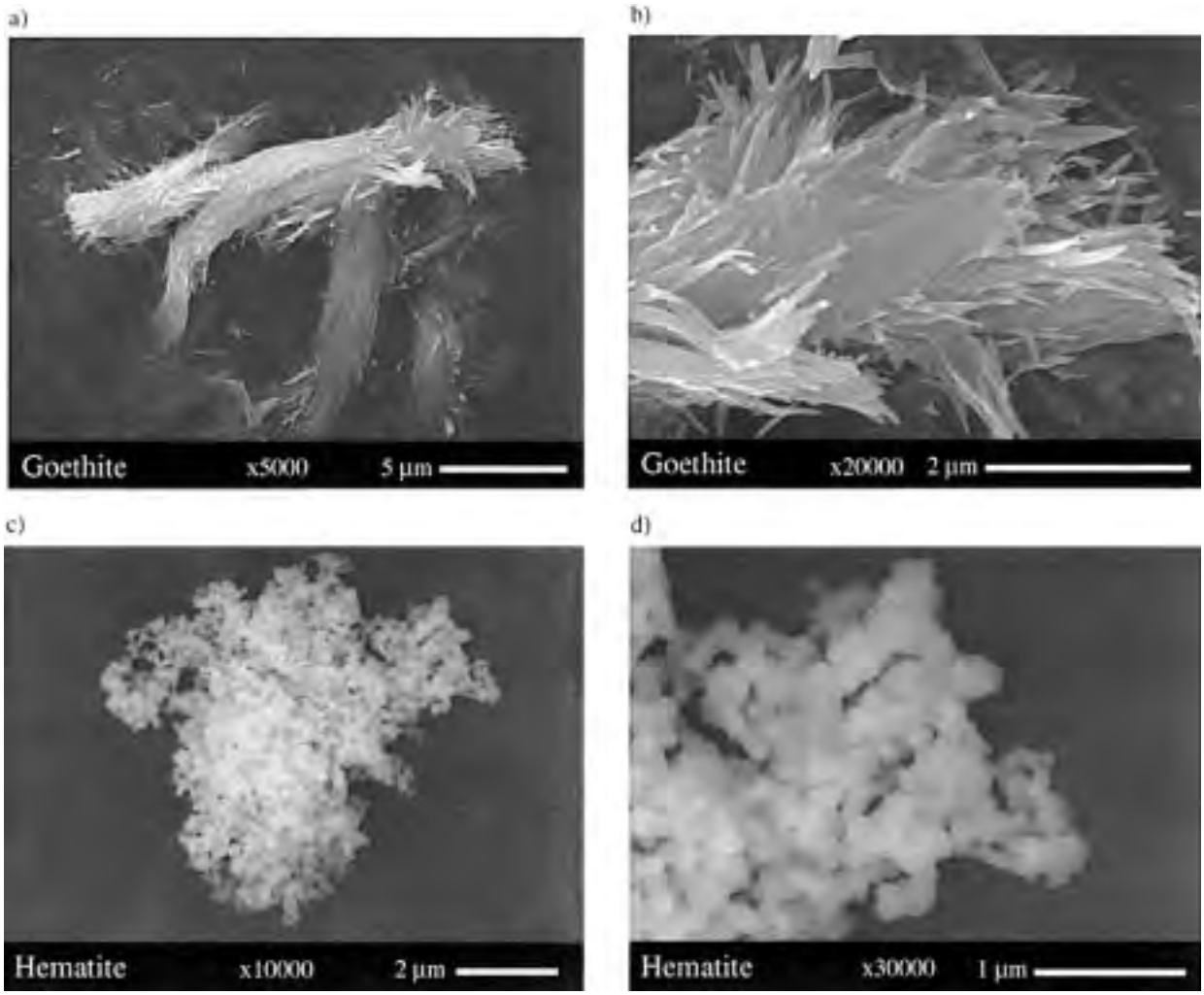

FIGURE 3. Field emission scanning electron micrographs of synthetic goethite (**a** and **b**) and hematite (**c** and **d**). Scale bars are variable as noted.

The extent of reduction (both without and with AQDS) in the Eatontown materials (10.0–28.7%, Table 4), was similar to that noted for synthetic goethite (9.2–32.8%, Table 2). However, a much greater percentage of the DCB extractable Fe^{3+} was reduced by CN32 in the Oyster and Milford sediments. Almost all the Fe^{3+} in the Milford sediment was bioreducible (Table 4). CN32 reduced crystalline Fe^{3+} oxides in the geologic materials because the amounts of poorly crystalline Fe^{3+} oxides, as defined by $NH_2OH{\cdot}HCl$ or ammonium oxalate extraction, in all of these sediments were low (Table 3).

In absence of PO_4, the $Fe^{2+}_{(aq)}$ concentrations increased with increasing amounts of bioreduction (Fig. 6b). When PO_4 was present, $Fe^{2+}_{(aq)}$ concentrations were uniformly lower, ranging between 0.3–0.6 m*M* (Fig. 6b), and tended to decrease with incubation time and amount of Fe^{2+} evolved (with the exception of the Eatontown hematite). Aqueous PO_4 concentrations measured immediately following inoculation indicated only a small amount of P was sorbed, with most PO_4 remaining in the aqueous phase (Fig. 7, day 0). With time and bioreduction, however, PO_4 concentrations generally decreased (Fig. 7, days 4, 11, and 27). The extent of PO_4 loss was qualitatively related to Fe^{2+} generation.

Mineralogic alterations. Biogenic alteration of the natural Fe^{3+} oxides was investigated for the Milford and Eatontown hematite sediments. The bioreducibility of the Fe^{3+} oxide fraction of these two sediments was different (Table 4). The Milford exhibited the highest Fe oxide fractional reduction (e.g., 100% with AQDS, Table 4), whereas the Eatontown showed the largest overall amount of reduction [e.g., 10.5 m*M* of HCl-Fe^{2+}, Table 4]. An oxide containing fine fraction was removed from the predominantly quartz sand matrix of both sediments by suspending them in 0.001 mol/L $NaClO_4$ and adjusting the pH to 8 with NaOH. This pH adjustment dispersed fine-grained oxide and clay particle coatings from the sand grains and allowed the collection of these separates by

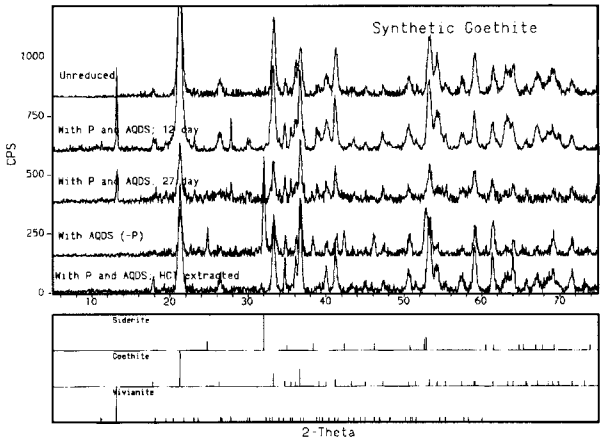

FIGURE 4. X-ray diffractograms (XRD) of unreduced goethite, and goethite subjected to bioreduction by CN32 under the noted conditions. Shown also is the XRD of a bioreduced goethite after HCl-extraction. Diffraction files for reference phases shown for comparison. (CPS = counts per second.)

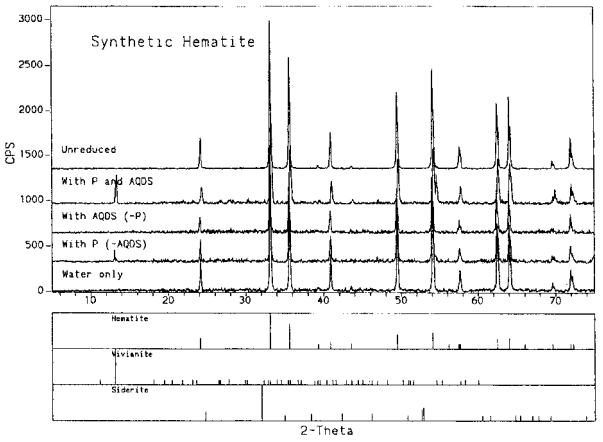

FIGURE 5. X-ray diffractograms (XRD) of unreduced hematite, and hematite subjected to bioreduction by CN32 under the noted solution conditions. Diffraction files for reference phases shown for comparison.

sedimentation. The separates were dialyzed against deionized water and freeze-dried.

The Milford separate contained kaolinite, quartz, and goethite as primary mineralogic components (Fig. 8). Its XRD pattern was complex with significant peak overlap that complicated phase identification, and broadening suggestive of submicrometer crystallites of phyllosilicates and possibly Fe^{3+} oxides. On average, the material consisted of micrometer-sized particle aggregates (Fig. 9a). The backscattered Fe images of these were diffuse, suggestive of nano-particulate Fe^{3+} oxides in mixture with other mass dominant phases. The EDS spectrum of the analyzed area (Fig. 9b) was typical of this material showing presence of Fe, but also that of Ti, Al, and Si; the latter elements being components of kaolinite that was the major mineral phase identified by XRD (Fig. 8). Higher magnification of the analyzed region showed the platey texture of the fundamental particles that were $<$100 to 400 nm. The aggregated material appeared as a matrix of fine-grained aluminosilicates and Fe oxides; however, discrete Fe^{3+} oxides were not identified.

The Eatontown hematite material (Fig. 10) yielded a more defined XRD pattern with all peaks resolved as mixture of quartz and hematite, with some goethite, mica, and kaolinite. Hematite particles were easily isolated and characterized in separates from the Eatontown hematite sediment. The particles were located by their backscattered image on SEM (not shown). Occasionally, the oxides were aggregated with kaolinite, but free, spherically shaped hematite particles (Fig. 11a) were the norm. The geologic hematite in the Eatontown sediment was larger in size ($\approx$0.85 μm) than the synthetic hematite (Fig. 3a). The geologic hematite contained Al and Si (Fig. 11b), and a highly textured surface (Fig. 11c).

The bioreduction experiment with the oxidic subsurface separates was conducted much like that for the specimen hematite and goethite. The masses of material were adjusted to yield suspension concentrations of 36 m*M* Fe^{3+} for the Milford separates and 50 m*M* Fe^{3+} for the Eatontown hematite separates, based on DCB extraction results. The maximum amount of Fe^{3+} reduced in the Milford separates after 27 days of incubation (13.0 m*M*, Table 5) was greater than observed for the whole sediment (4.61 m*M*, Table 4), but the fractional reduction was less (36.2% as compared to approximately 100%) (Tables 4 and 5). In general, less Fe^{3+} was reduced in the Eatontown separates (4.6–9.5 m*M)* than in the Milford separates (8.0–13.0 m*M),* Table 5. The maximal extent of Fe^{2+} production in the Eatontown separates was similar to that noted in the whole sediment (e.g., 9.53 m*M* as compared to 10.5 m*M),* but the fractional reduction was also less (e.g., 19.1% compared to 28.7%), as noted for the Milford separates. The fractional reducibility, or bioavailability, of the oxide fraction in the sediments is therefore not a constant value. It appears dependent on the concentration of the Fe^{3+} oxides (i.e., surface area) relative to the microbial population size. Roden and Zachara (1996) noted a similar effect and attributed it to an absorption effect of the smaller oxide particles on the microorganism surface. The organism surfaces may, themselves, become saturated with oxide particles, preventing further contact with other particles.

The XRD patterns of the reduced separates did not show major mineralogic change from the starting materials (Figs. 12 and 13). There was a slight but noticeable decrease in peak intensity of the crystalline oxides (e.g., goethite and hematite) after microbial reduction. Crystalline reduction products were not observed in the Milford separates, although the degree of reduction (13.0 m*M* Fe^{2+}-HCl at maximum) was similar in magnitude to that of goethite (e.g., 16.4 m*M,* Table 2) where both vivianite and siderite were observed (Fig. 4). Vivianite formation was observed in the Eatontown hematite separates in the

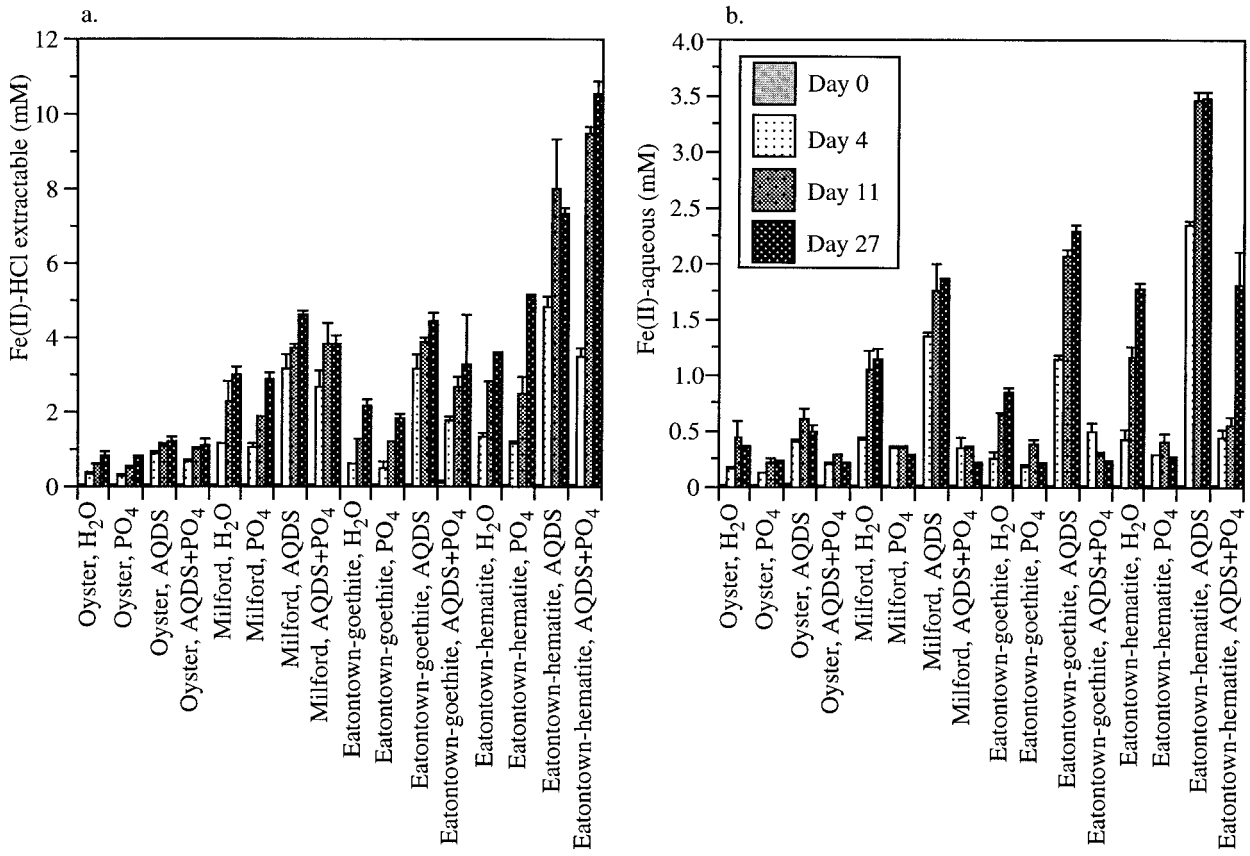

FIGURE 6. HCl-extractable (**a**) and aqueous Fe^{2+} (**b**) observed in bioreduction experiments with subsurface sediments and CN32 in bicarbonate buffer. Results show the impact of AQDS and PO_4.

treatment that produced the greatest extent of reduction [P+AQDS, 9.53 m*M* Fe^{2+}, Fig. 13]. There was no evidence for siderite formation (within the degree of sensitivity of XRD) in the geologic separates in spite of 30 m*M* bicarbonate. Magnetite was also not observed.

Substrate and population dynamics. The lactate-driven bioreduction of goethite (FeOOH) and hematite (Fe_2O_3) may be described analogously:

$$4FeOOH + CH_3CHOHCOO^- + 7H^+ = 4Fe^{2+} + CH_3COO^- + HCO_3^- + 6H_2O \quad (1)$$

$$2Fe_2O_3 + CH_3CHOHCOO^- + 7H^+ = 4Fe^{2+} + CH_3COO^- + HCO_3^- + 4H_2O \quad (2)$$

Acetate (CH_3COO^-) is produced at a molar ratio of 1:4, acetate to Fe^{2+}. Acetate was measured after 27 d of incubation and its concentration with respect to Fe^{2+} followed the expected molar ratio in Equations 1 and 2 (Fig. 14), although variability was noted. The results indicated that the reduction of crystalline Fe^{3+} oxides in the subsurface materials was the primary pathway for microbiologic electron disposal during respiration of lactate.

Previous studies have shown that *Shewanella* strains can grow using goethite (Roden and Zachara 1996) and magnetite (Kostka and Nealson 1995) as electron acceptors. Cell numbers were determined in the bioreduction experiments with geologic materials after 4, 11, and 27 d of incubation using acridine orange staining and epifluoresence microscopy. Cell densities were quite uniform throughout all treatments (data not shown) with an average of $(2.0 \pm 0.1) \times 10^8$ CN32 cells/mL, regardless of whether media conditions were or were not growth supporting (i.e., with or without P). The direct counts indicated that growth was minimal, or at least not discernable given the high initial cell concentration.

DISCUSSION

The experimental results define three major findings: (1) AQDS enhances the bioreduction of both synthetic and natural Fe^{3+} oxides but the effects are more pronounced on the synthetic ones, (2) both vivianite and siderite are biogenic products of dissimilatory reduction of synthetic and natural Fe^{3+} oxides in bicarbonate buffer, but vivianite formation precedes that of siderite, and (3) the subsurface Fe^{3+} oxides show differences in reducibility from the synthetic solids.

Role of AQDS

AQDS has been shown to mediate the bacterial reduction of HFO (Fredrickson et al. 1998; Lovley et al. 1996).

TABLE 3. Extractable Fe and Al and mineralogy of subsurface materials

	$NH_2OH \cdot HCl$* (μmol/g)		Am-Ox† (μmol/g)		DCB‡ (μmol/g)		Oxide§ Mineralogy	Surface‖ Area (m^2/g)
	Fe	Al	Fe	Al	Fe	Al		
Oyster	1.26	22.7	3.67	23.7	13.2	13.8	feroxyhyte	3.1
Milford	1.72	10.4	5.65	8.60	45.1	25.1	goethite	6.8
Eatontown goethite	0.18	0.40	0.66	0.76	183	21.2	goethite	1.4
Eatontown hematite	0.49	0.60	2.40	1.11	366	17.0	hematite/goethite	3.1

* Acidified hydroxyl-amine hydrochloride.
† Ammonium oxalate in the dark.
‡ Dithionite, citrate, and bicarbonate.
§ All crystalline Fe^{3+} oxides observed by XRD, whether major or minor in apparent concentration.
‖ Of the <2 mm sediment.

Ours, however, is the first report that AQDS also stimulates DMRB reduction of crystalline Fe^{3+} oxides.

AQDS can function as an electron acceptor/repository for microbial respiration by the following reaction:

$$AQDS + 2H^+ + 2e^- = AHDS \qquad E^0 = 0.23\ V \quad (3)$$

Note, both the oxidized (AQDS) and reduced forms (AHDS) carry a formal charge of 2^- contributed by the two sulfonate groups; AHDS is an acronym for the reduced species where both quinone groups have been reduced and protonated to phenolate groups. The mechanisms by which AQDS enhances the reduction rate of Fe oxides have not been established, but it is presumed that AQDS functions as an electron shuttle between the microbial electron transport chain and the oxide surface, and negates the need for direct organism-oxide contact. The organisms donate electrons to AQDS at the terminal point of the electron transport chain located in the periplasmic space or outer membrane (Myers and Myers 1992), reducing it to AHDS. Subsequently, AHDS forms a surface complex on the oxide surface that passes electrons to the Fe^{3+} metal ion center. AHDS enhances Fe^{3+} oxide reduction by gaining better accesses to complex interstices of the solid not readily accessible to immobile redox proteins on the bacterial surface.

Although studies have not been performed to document that AHDS promotes abiotic reductive dissolution of Fe^{3+} oxides, the behavior of a related compound (hydroquinone) has been studied (Kung and McBride 1988; LaKind and Stone 1989; Stone and Morgan 1984; Stone and Ulrich 1989). AHDS is expected to complex with the Fe^{3+} oxide surface in a manner similar to hydroquinone. Stone and coworkers found that the ability of hydroquinone to reductively dissolve Mn^{3+}, Mn^{4+}, Co^{3+}, and Fe^{3+} oxides was dependent on reaction thermodynamics and the effects of reduced metal sorption (Fe^{2+}, Mn^{2+}, and Co^{2+}) on the remaining oxide surface. Hydroquinone was an effective reductant of both Mn and Co oxide at circumneutral pH, but goethite and hematite were poorly dissolved (LaKind and Stone 1989; Stone and Ulrich 1989). Accordingly, the reduction potential (E′) of hydroquinone lies below that of the $Mn^{3+,4+}$ and Co^{3+} oxides above that of the crystalline Fe^{3+} oxides at neutral pH (Table 6).

AHDS, however, is a more powerful reductant than hydroquinone and should readily reduce HFO [e.g.,

TABLE 4. Bioreduction extent of Fe^{3+} oxide-containing subsurface sediments

Oxide	Fe^{2+}-HCl (m*M*)	% Reduced
Oyster, H_2O	0.81	61.4
Oyster, H_2O+PO_4	0.80	60.2
Oyster, AQDS	1.20	90.6
Oyster, AQDS+PO_4	1.08	81.7
Milford, H_2O	2.95	65.5
Milford, H_2O+PO_4	2.90	64.2
Milford, AQDS	4.61	100
Milford, AQDS+PO_4	3.81	84.5
Eatontown-goethite, H_2O	2.16	11.8
Eatontown-goethite, H_2O+PO_4	1.83	9.9
Eatontown-goethite, AQDS	4.44	24.3
Eatontown-goethite, AQDS+PO_4	3.24	17.7
Eatontown-hematite, H_2O	3.54	9.7
Eatontown-hematite, H_2O+PO_4	5.10	13.9
Eatontown-hematite, AQDS	7.30	19.9
Eatontown-hematite, AQDS+PO_4	10.5	28.7

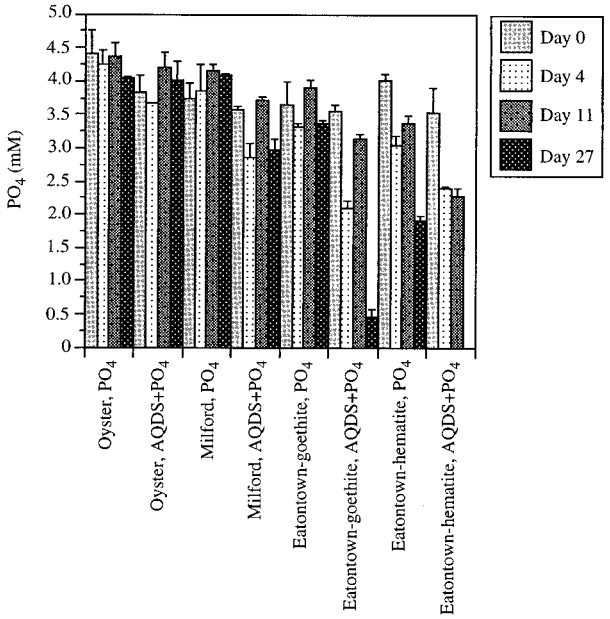

FIGURE 7. Soluble PO_4 in the bioreduction experiments with subsurface sediments.

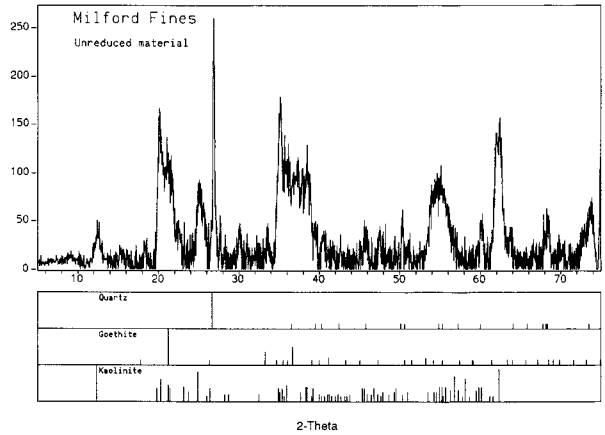

FIGURE 8. X-ray diffractogram of unreduced Milford separates, with card file data for reference phases.

$Fe(OH)_{3(s)}$, Table 6] at circumneutral pH. Furthermore, its reaction with goethite or hematite is potentially favorable as its reduction potential lies immediately below that of the crystalline Fe^{3+} oxides at pH 7 under the other assumed conditions of calculation (e.g., $[Me^{2+}]$ and [AQDS/AHDS]). The close parity in reduction potentials (E′) of the AQDS and the crystalline Fe^{3+} solids (Table 6) indicates that the relative ability of AHDS to function as a reductant is strongly dependent on the thermodynamic properties of the solid phase Fe^{3+} oxides, the $[Fe^{2+}]$, and the degree of reduction of AQDS promoted by microbial respiration. The fact that AQDS promotes the bacterial reduction of HFO and the crystalline oxides indicates it is a preferred, or possibly more facile electron acceptor for DMRB than is the Fe^{3+} oxide surface. These observations and spectroscopic measurements by Fredrickson et al. (1998) indicate that AQDS is converted to AHDS by active DMRB under anoxic conditions.

Biogenic mineralization

Fe reduction in the bacterial system studied here is driven by the microbial liberation of reductive equivalents in lactate, the electron donor (Eqs. 1 and 2). Fe^{3+} oxides, and AQDS to a lessor degree, serve as a electron repository/acceptor and are reduced by the terminal reductase or other electron transfer agents at the cell surface. A decrease in system pe (opposite log of electron activity) follows lactate metabolism and electron liberation. Figure 15 displays the computed stability of goethite and hematite [at 50 m*M* Fe^{3+}] as a function of pe in the 30 m*M* bicarbonate buffer with 4 m*M* P and the other media components listed in Table 1. The computation was performed with the MINTEQA2 code incorporating aqueous complexation reactions of sulfate, bicarbonate/carbonate, phosphate, acetate, and lactate at the average values noted in experiment (e.g., pH 6.9 and I = 0.1).

Goethite is less stable than hematite and, hence, dissolves at a higher pe (≅1.8). This observation was, in part, consistent with experiment where synthetic goethite

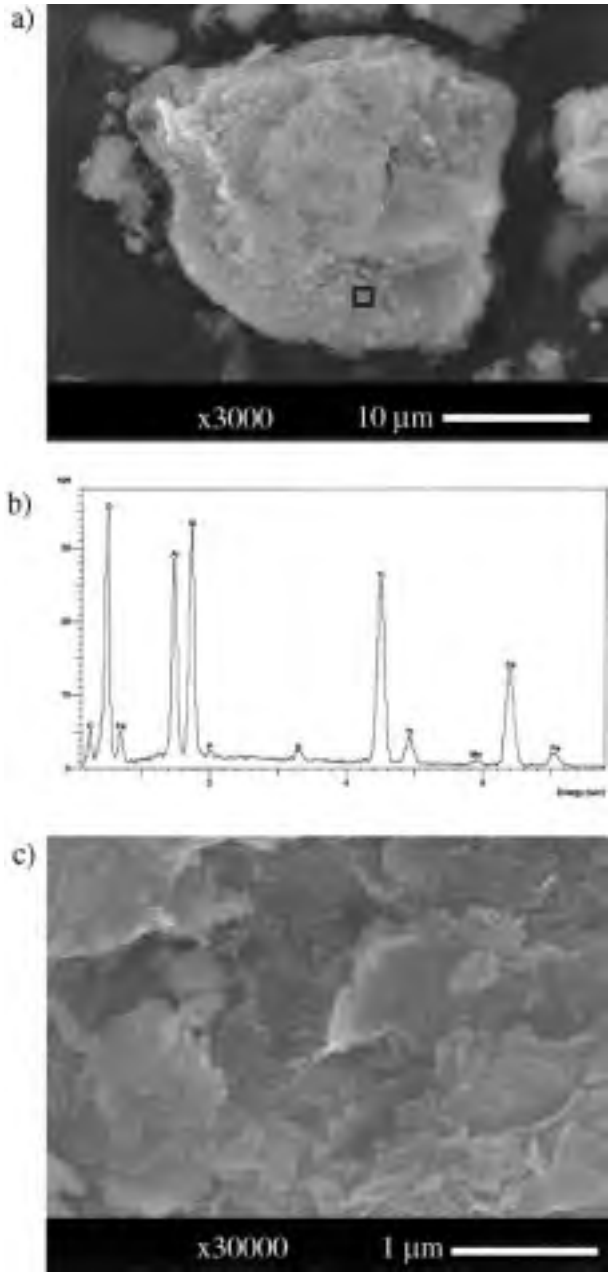

FIGURE 9. Scanning electron micrograph of an average particle aggregate from the Milford separates (**a**), the EDS spectra of the noted point that showed average properties (**b**), and higher magnification of the surface at the analyzed point (**c**).

was found to be reduced to a greater extent by CN32 than was synthetic hematite (Table 2). Free energy data indicate that vivianite should be the initial phase to precipitate as Fe^{2+} is produced, as its solubility (in presence of 4 m*M* P) is lower than siderite. Experiment confirmed this prediction (Figs. 4, 5, and 13). In both the goethite and hematite systems, siderite precipitation was predicted to commence when soluble P was fully incorporated into vivianite. In contrast to the experimental result, however,

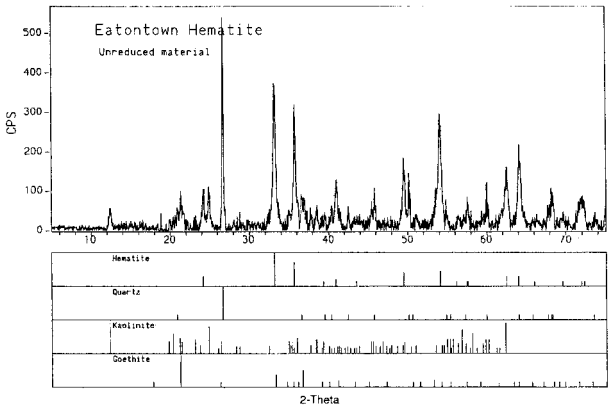

FIGURE 10. X-ray diffractogram of unreduced Eatontown hematite, with card file data for reference phases.

the thermodynamic calculation suggests that goethite and hematite should fully dissolve to yield siderite when the pe reaches the requisite value (e.g., −1.75 for goethite and −4.0 for hematite). Possible reasons for these discrepancies will be discussed later. This full predicted transformation of the Fe^{3+} oxide to Fe^{2+} carbonate is driven by the high total carbonate concentration of the system (10^{-2} mol/L in solution and 20% $CO_{2(g)}$ in the headspace).

Vivianite appears to form readily in sediments (Emerson and Widmer 1978; Postma 1981; Suess 1979) and our observations indicate it exhibits rapid precipitation rates in batch bioreduction experiments. Parallel to our study, the paragenesis of vivianite and siderite in bog sediment was predictable from thermodynamic considerations such as those in Figure 15 (Postma 1981). The relationship between total Fe^{2+} and aqueous PO_4 in the bioreduction experiments of goethite and hematite with P (both with and without AQDS) closely followed that of a vivianite-siderite precipitation model (Fig. 16). Model calculations were generated by metering Fe^{2+} into the P-containing (3.5 m*M),* bicarbonate (35 m*M)* buffered solution at pH 6.9 and I = 0.1 (I = ionic strength), and allowing siderite and vivianite to precipitate when saturation was exceeded. In that calculation, vivianite was found to precipitate as a single discrete phase until P concentrations were exhausted [$Fe^{2+} \approx 5$ m*M*]. Above that Fe^{2+} concentration, siderite precipitated in association with the vivianite. This precipitation sequence created the two distinct linear sections in Figure 16.

Results from the sediment bioreduction experiments qualitatively followed the vivianite-siderite model (Fig. 16). However, higher concentrations of 0.5 N HCl-extractable Fe^{2+} were required in the sediments to achieve comparable reductions in $PO_{4(aq)}$. This difference resulted from the higher $PO_{4(aq)}$ concentrations used in the latter experiments (4.5 m*M*, Fig. 7), and the possible effects of Fe^{2+} sorption to accessory phases in the sediments (e.g., kaolinite). We conclude from Figure 16 that the vivianite-siderite phase association is a reasonable first order model of the biomineralization processes in the oxide and sediment bioreduction experiments, and that the limited sensitivity of XRD (e.g., phases at less than 5 mass percent are not readily resolved) prevented direct identification of these phases in those experiments where bioreduction was more limited.

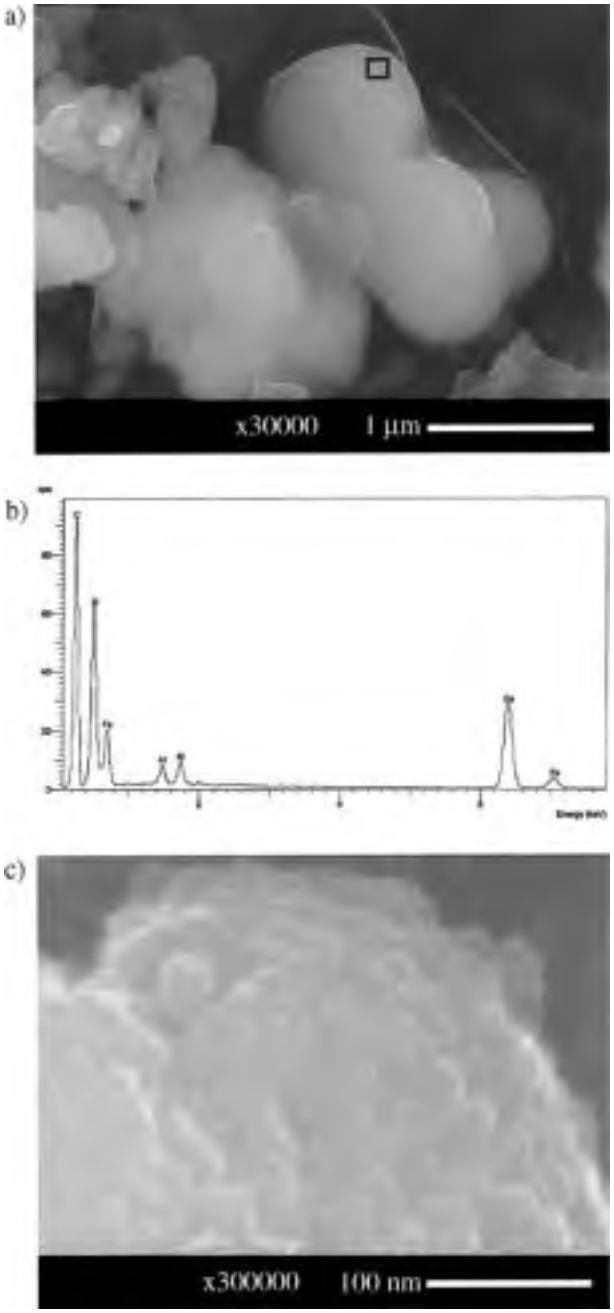

FIGURE 11. Scanning electron micrograph of unreduced hematite particles from the Eatontown hematite sediment (**a**), the elemental analysis of the noted spot by EDS (**b**), and a higher magnification view of the natural oxide surface (**c**).

The noted coexistence of goethite along with siderite (Fig. 4) in presence of excess electron donor (lactate) was one clear experimental indication of system disequilibria

TABLE 5. Bioreduction of Fe^{3+} oxide separates from Atlantic Coastal Plain subsurface sediments in bicarbonate buffer after 27 d incubation

Solids	Media	Final pH	$[Fe^{2+}]_{aq}$ (mmol/L)	$[Fe^{2+}$-HCl] (mmol/L)	% Fe^{3+} Reduced
Eatontown hematite separate*	P + AQDS	7.44	0.63	9.53	19.1
Eatontown hematite separate*	AQDS (-P)	7.23	2.52	6.39	12.8
Eatontown hematite separate*	P (-AQDS)	7.18	0.14	4.58	9.16
Milford separates†	P + AQDS	6.88	0.92	13.0	36.2
Milford separates†	AQDS (-P)	6.65	1.34	10.5	29.1
Milford separates†	P (-AQDS)	6.73	0.33	7.99	22.2

* 50 m*M* Fe^{3+} starting concentration.
† 36 m*M* Fe^{3+} starting concentration.

(i.e., compare to Fig. 15) at experiment termination. This assessment was not as easily made for hematite, because siderite was not observed in the bioreduction experiments and the noted association of vivianite and hematite (Fig. 5) was consistent with thermodynamic prediction between pe = −3.2 to −4.2 (Fig. 15). Roden and Zachara (1996) speculated that passivation of crystalline oxide surfaces with sorbed, biogenic Fe^{2+} prevented full microbial utilization of Fe^{3+} in goethite and hematite suspensions. Abiotic analogues of this phenomena exist. For example, surface passivation of magnetite by maghemite prevents chromate reduction that otherwise proceeds rapidly on the clean magnetite surface (Peterson et al. 1996). More recent experiments on DMRB reduction of crystalline Fe^{3+} oxides, however, bring the Fe^{2+} surface passivation hypothesis into question. Urrutia et al. (1998) found that *S. alga* re-inoculated into Fe^{3+} oxide culture or into oxide suspensions with Fe^{2+} preadsorbed to oxides at saturation levels were able to reduce significant amounts of Fe^{3+} associated with a synthetic goethite. These results suggest that other complex and interactive factors including biosorption and organism physiology may also be significant.

Surface area and other factors controlling reducibility of natural Fe^{3+} oxides

Goethite and hematite have been used herein as models of the crystalline Fe^{3+} oxide fraction in subsurface sediment. The bioreducibility of the synthetic goethite and the goethite in the Milford separates was similar (Table 7), whereas the synthetic hematite and the Eatontown hematite were less comparable. Generally, the geologic oxides were equally or more reducible than their synthetic counterparts. In a previous communication (Roden and Zachara 1996) we found that the degree of reducibility, or bioavailability, of a series of synthetic Fe^{3+} oxides followed in direct proportion to their surface area. Hematite had the lowest surface area and fractional reducibility, whereas HFO had the greatest. We questioned whether morphology and particle size differences between the synthetic and subsurface oxides might explain the noted behaviors here.

Whereas the noted dependence of synthetic Fe^{3+} oxide bacterial reducibility on surface area is intuitive given the heterogeneous nature of the reaction, it may be an oversimplification. An issue is whether all the measured surface area is, or can ever be available to the much larger microorganism, and whether microbial induced aggregation occurs. Figure 3 shows that the fundamental crystal-

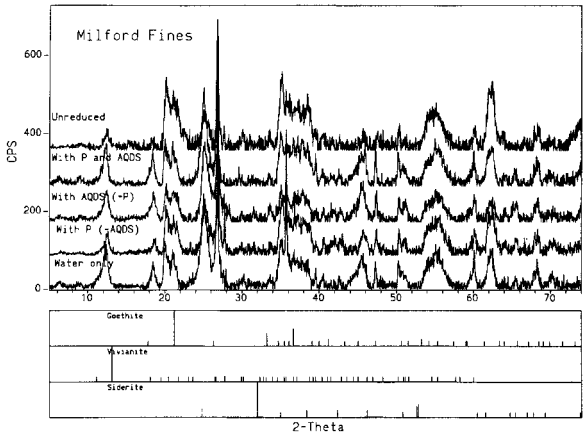

FIGURE 12. X-ray diffractograms of the unreduced and bioreduced Milford separates under noted solution conditions.

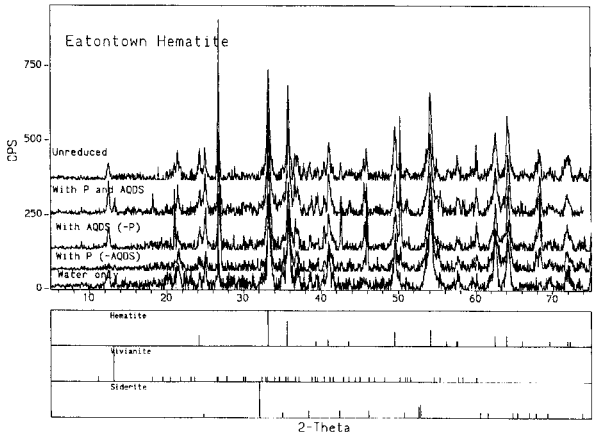

FIGURE 13. X-ray diffractograms of the unreduced and bioreduced Eatontown hematite under noted solution conditions.

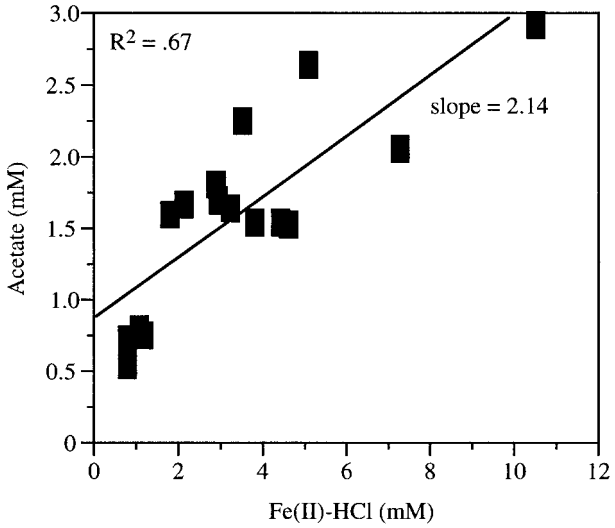

FIGURE 14. Relationship of acetate generation to Fe^{3+} reduction in the various media, AQDS, and PO_4 treatments with the subsurface sediments.

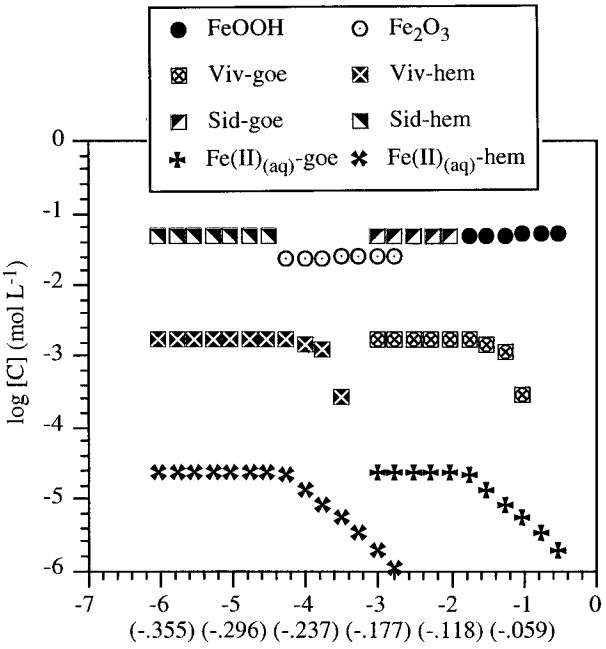

FIGURE 15. Thermodynamic calculations of goethite and hematite stability as a function of pe in the bicarbonate buffered basal media. [C] is the concentration of the different solid [FeOOH, Fe_2O_3, $FeCO_3$, and $Fe_3(PO_4)_2 \cdot 8H_2O$] and aqueous species (Fe^{2+}) in moles per liter. Viv-goe, Sid-goe, and $Fe^{2+}_{(aq)}$-goe represent the concentrations of $Fe_3(PO_4)_3 \cdot 8H_2O$, $FeCO_3$, and $Fe^{2+}_{(aq)}$ in equilibrium with goethite at the noted pe. Viv-hem, sid-hem, and $Fe^{2+}_{(aq)}$-hem are defined, accordingly, for hematite. The initial oxide concentrations in the calculation were 0.025 mol/L hematite (50 m*M* as Fe^{3+}) and 0.050 mol/L goethite (50 m*M* as Fe^{3+}).

lite size of the hematite and goethite are comparable at 300–500 nm, yet their surface areas differ by a factor of ten with hematite being smaller. The higher surface area of goethite may result from surface roughness or serrated edges (Cornell and Schwertmann 1996) and internal microporosity, although the existence of microporosity in acicular goethite is debatable (Naono and Figiwara 1980; Naono et al. 1987; Torrent et al. 1990). Spherical hematite lacks marked surface roughness (especially if calcined) and interparticle porosity (Cornell and Schwertmann 1996), and its measured and calculated surface areas often coincide (Kandori et al. 1991). The surface area of HFO is difficult to establish, and reported values range between 300–700 m^2/g depending on age, preparation, and measurement method (Cornell and Schwertmann 1996; Dzombak and Morel 1990). The fundamental HFO particles (ca. 5 nm) readily form aggregates > 0.1 μm (Cornell and Schwertmann 1996) with significant interparticle porosity (Crosby et al. 1983) that may change with aging (Weidler 1995) and temperature (Cornejo 1987).

The data in Figure 1 was not fully normalized by surface area (Fig. 17). Goethite and hematite were reduced comparably on a surface area basis in the absence of AQDS as reported previously (Roden and Zachara 1996), but this similarity decreased when AQDS was present. The increased reduction of hematite over goethite with AQDS was not expected. Rather, it was assumed that reduced AQDS would render goethite more available by

TABLE 6. Reduction potentials of benzoquinone (Q) and AQDS relative to metal oxides

Half-reaction	E°*	E′†	Source
$1/2Mn^{4+}O_{2(s)} + 2H^+ + e^- = 1/2Mn^{2+} + H_2O$	+1.29	+0.64	Stone and Ulrich 1989
$Mn^{3+}OOH_{(s)} + 3H^+ + e^- = Mn^{2+} + 2H_2O$	+1.50	+0.61	Stone and Ulrich 1989
$CoOOH_{(s)} + 3H^+ + e^- = Co^{2+} + 2H_2O$	+1.48	+0.59	Stone and Ulrich 1989
$1/2Q + H^+ + e^- = 1/2HQ$‡	+0.70	+0.23	Stone and Ulrich 1989
$Fe(OH)_3 + 3H^+ + e^- = Fe^{2+} + 3H_2O$	+1.06	+0.17	Lindsay 1979
$FeOOH_{(s)} + 3H^+ + e^- = Fe^{2+} + 2H_2O$	+0.67	−0.22	Stone and Ulrich 1989
$1/2Fe_2O_{3(s)} + 3H^+ + e^- = Fe^{2+} + 3/2H_2O$	+0.66	−0.23	Stone and Ulrich 1989
$1/2AQDS + H^+ + e^- = 1/2AHDS$	+0.23	−0.24	Clark 1960

* E° = standard reduction potential.
† E' = reduction potential with $[H^+] = 1.0 \times 10^{-7}$ mol/L, $[Me^+] = 1.0 \times 10^{-6}$ mol/L, [Q, AQDS] $= 1.0 \times 10^{-6}$ mol/L and [HQ, AHDS] $= 1.0 \times 10^{-4}$ mol/L.
‡ HQ = hydroquinone.

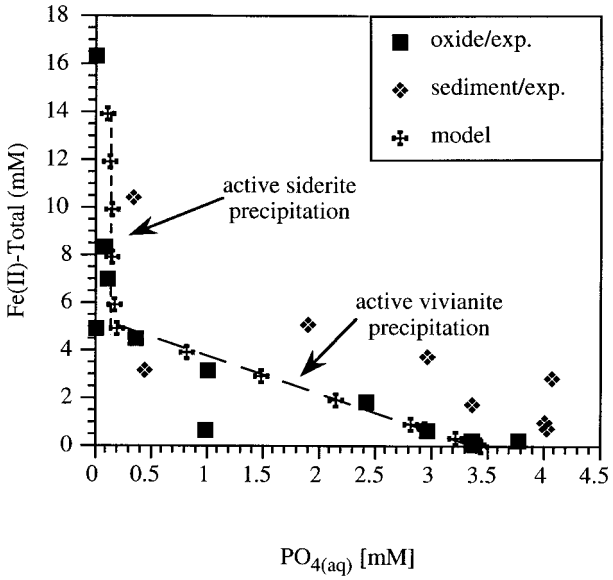

FIGURE 16. Model and experimental data on the relationship of total Fe^{2+} [eg., 0.5N HCl extractable] to aqueous phosphate. Shown are data from the oxide (Figs. 1a and 2b) and sediment incubations (Figs. 5d and 6b) at experiment termination. The model results were obtained by numerically metering Fe^{2+} into the P-containing (3.5 m*M)* bicarbonate buffered media (pH 6.9, I = 0.1) and allowing vivianite or siderite to precipitate according to thermodynamic constraint. The plotted value of PO_4 is that remaining in solution after addition of the noted total concentration of Fe^{2+}. The model results define a region of active siderite precipitation ($PO_4 < 0.2$ m*M)* and one of active vivianite precipitation ($PO_4 > 0.2$ m*M).*

accessing microtopographic features and microporous regions along grain boundaries, etc., that were implied by the surface area measurement and were not in position to easily contact the microorganism surface. Experiment replication indicated that the result with hematite and AQDS was not spurious, although repeat results varied significantly (±20%) within the range discussed previously (Fredrickson et al. 1998). HFO was markedly less reducible than either hematite or goethite when 550 m^2/g was used as the estimated surface area. The HFO in these experiments was autoclaved. Heating HFO changes its aggregate and pore structure (Cornejo 1987), reduces surface area (Stanjek and Weidler 1992), and may induce transformation to hematite (Cornell and Schwertmann 1996; Stanjek and Weidler 1992) that PO_4 acts to retard (Fredrickson et al. 1998). Thus, the surface area used for normalization may be in error for HFO, with a smaller value being more appropriate. In spite of these potential effects of heat on HFO properties, however, Fredrickson et al. (1998) saw little effect of autoclaving on the bioreduction of HFO by CN32. Given the noted questions and uncertainties, a more detailed evaluation (both with and without AQDS) of the relationship between bacterial dissolution and Fe^{3+} oxide surface area appears warranted.

TABLE 7. Comparison of bioreduction of synthetic and natural oxides

Solid	Treatment	[Fe^{3+}]	% Reduced
Goethite	P + AQDS	50 m*M*	32.8
	AQDS (-P)	50 m*M*	35.0
	P (-AQDS)	50 m*M*	9.2
Milford Fines*	P + AQDS	36 m*M*	36.2
	AQDS (-P)	36 m*M*	29.1
	P (-AQDS)	36 m*M*	22.2
Hematite†	P + AQDS	50 m*M*	6.8
	AQDS (-P)	50 m*M*	3.9
	P (-AQDS)	50 m*M*	1.40
Eatontown Hematite‡	P + AQDS	50 m*M*	19.1
	AQDS (-P)	50 m*M*	12.8
	P (-AQDS)	50 m*M*	9.2

* Goethite is the primary Fe^{3+} oxide.
† Second experiment X-ray diffraction collected (Fig. 5).
‡ Hematite is the primary Fe^{3+} oxide.

Dissolution studies with synthetic Fe^{3+} oxides have shown that dissolution rate is controlled by various interrelated factors that are often difficult to resolve including surface area; morphology; crystal habit; microheterogeneities such as point defects, dislocations, microfractures, domain boundaries, corners, ledges, etc.; internal order; and minor element substituents (Cornell and Schwertmann 1996). These factors have contrasting effects. For example, the presence of microheterogeneities and internal disorder increases dissolution rate (e.g., Schwertmann et al. 1985) whereas Al substitution, a common feature of geologic and soil goethites and hematite, slows dissolution (Norrish and Taylor 1961; Schwertmann 1984; Torrent et al. 1987).

The dissolution behavior of natural oxides is complicated by variations in all the above noted factors, and indeed Schwertmann (1991) was unable to correlate the

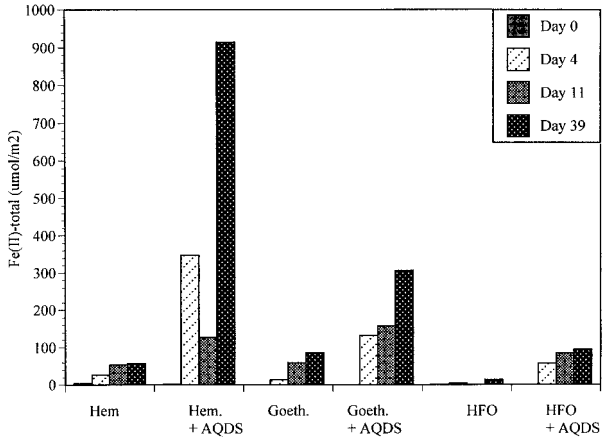

FIGURE 17. Total biotic Fe^{2+} generation in synthetic Fe^{3+} oxide suspensions (from Fig. 1a) normalized to surface area. Surface areas used: HFO = 550 m^2/g, goethite = 52.3 m^2/g, and hematite = 5.2 m^2/g.

acid dissolution rates of a series of natural Fe oxides with measurable properties such as surface area and Al-substitution. We observed that Fe^{3+} oxides in the Milford separate exhibited comparable bacterial reducibility to synthetic goethite in spite of their apparent smaller size. In contrast, the geologic hematite (Eatontown) seemed more reducible than its synthetic counterpart, in spite of larger crystallite size. Aluminum concentrations in DCB extractions (not shown) and Mössbauer and XRD measurements (Zachara, unpublished data) of the Milford and Eatontown separates both imply that the geologic Fe^{3+} oxides are Al-substituted, although the concentration degree has not yet been established. The differential behavior of the geologic and synthetic Fe^{3+} oxides observed herein is not resolvable with current data, but is likely influenced by Al-substitution and other factors related to crystallite order and defects. The presence of associated mineral phases that may adsorb biogenic Fe^{2+} in the geologic Fe^{3+} oxide separates may also have an unknown influence on both dissolution rate, extent, and biomineralization.

It was noted (Fig. 17) that synthetic hematite is equally bioreducible to goethite on a surface area basis, and may be even more reducible than goethite in presence of an electron shuttle (AQDS), reasons unknown. Furthermore, the geologic hematite (Eatontown) was more reducible than expected given its relatively large crystallite size (ca. 0.85 μm, Fig. 11). These findings seem consistent with color changes (yellowing/xanthization) observed during reduction of goethitic/hematitic soils (Cornell and Schwertmann 1996; Jeanroy et al. 1991) that are thought to result from the preferential dissolution of soil hematite over goethite. The cause for such preferential dissolution has not been determined, but is speculated to result from the inhibitory effect of Al-substitution on goethite, as soil goethite typically shows greater Al content. Our results suggest, however, that other properties of geologic/soil hematite, such as disorder or microheterogeneities (e.g., Fig. 11c), may enhance its reducibility over synthetic phases.

Conclusions

S. putrefaciens, CN32, was effective in reducing synthetic and geologic crystalline Fe^{3+} oxides. Except in limited cases where Fe^{3+} oxides were in low concentration in geologic materials, the oxides were not reduced to completion in presence of excess electron donor suggesting chemical or physiologic controls on bioavailability. Vivianite and siderite were the primary crystalline products of Fe^{3+} oxide bioreduction. Both phases precipitated readily in our experimental systems, and the conditions of their formation were consistent with published solubility values. It was not established, however, whether the microorganisms acted to nucleate or direct the precipitation of these secondary phases. The geologic Fe^{3+} oxides were more reducible than their synthetic counterparts, possibly as a result of crystallinity differences or microheterogeneities. *S. putrefaciens* demonstrated remarkable ability to access Fe^{3+} oxides in complex mineral composites, as shown with the Milford fines. Precisely how the microorganisms differentiate and isolate the Fe^{3+} oxides in a mixture of mineral phases and what controls the bioavailability of the Fe^{3+} oxide once found are important biogeochemical questions that beg resolution.

Acknowledgments

This research was supported by the Natural and Accelerated Bioremediation Research Program (NABIR), Office of Biological and Environmental Research (OBER), and U.S. Department of Energy (DOE). The continued support of F.J. Wobber is appreciated. Geologic materials used in this paper were taken from the NABIR subsurface sediment collection, and the support of this collection by the NABIR Field Research Center (FRC) and Paul Bayer is appreciated. The helpful comments of two anonymous reviewers are also appreciated.

References cited

Al-Borno, A. and Tomson, M.B. (1994) The temperature dependence of the solubility product constant of vivianite. Geochimica et Cosmochimica Acta, 58, 5373–5378.

Allison, J.D., Brown, D.S., and Novo-Gradac, K.J. (1991) MINTEQA2/PRODEFA2, A Geochemical Assessment Model for Environmental Systems: Version 3.0 User's Manual. no. U.S. Environmental Protection Agency, Athens, Georgia.

Arnold, R.G., DeChristina, T.J., and Hoffman, M.R. (1988) Reductive dissolution of Fe^{3+} oxides by *Pseudomonas* sp. 200. Biotechnology and Bioengineering, 32, 1081–1096.

Baedecker, M.J., Cozzarelli, I.M., Evans, J.R., and Hearn, P.P. (1992) Authigenic mineral formation in aquifers rich in organic material. In Kharaka and Maest, Eds., Water-Rock Interaction, p. 257–261. Balkema, Rotterdam.

Bruno, J., Wersin, P., and Stumm, W. (1992) On the influence of carbonate in mineral dissolution: II. The solubility of $FeCO_3$ (s) at 25 °C and 1 atm total pressure. Geochimica et Cosmochimica Acta, 56, 1149–1155.

Chao, T.T. and Zhou, L. (1983) Extraction techniques for selective dissolution of amorphous Fe oxides from soils and sediments. Soil Science Society of America Journal, 47, 225–232.

Chapelle, F.H. (1993) Ground-Water Microbiology and Geochemistry. Wiley, New York.

Chapelle, F.H. and Lovley, D.R. (1992) Competitive exclusion of sulfate reduction by Fe^{3+}-reducing bacteria: a mechanism for producing discrete zones of high-Fe ground water. Ground Water, 30, 29–36.

Clark, W.M. (1960) Oxidation-Reduction Potentials of Organic Systems. The Williams and Wilkins Co., Baltimore, Maryland.

Coates, J.D., Lonergan, D.J., Philips, J.P., Jenter, H., and Lovley, D.R. (1995) *Desulfuromonas palmitatis* sp. nov., a marine dissimilatory Fe^{3+} reducer that can oxidize long-chain fatty acids. Archives Microbiology, 164, 406–413.

Colombo, C., Barron, V., and Torrent, J. (1994) Phosphate adsorption and desorption in relation to morphology and crystal properties of synthetic hematites. Geochimica et Cosmochimica Acta, 58, 1261–1269.

Cornejo, J. (1987) Porosity evaluation of thermally treated hydrous oxide gel. Journal Colloid Interface Science, 115, 260–263.

Cornell, R.M. and Schwertmann, U. (1996) The Fe Oxides: Structure, Properties, Reactions, Occurrences, and Uses. VCH, Weinheim, 573.

Crosby, S.A., Glasson, D.R., Cuttler, A.H., Butler, I., Turner, G.T., Whitefield, M., and Millward, G.E. (1983) Surface areas and porosities of Fe^{3+}-and Fe^{2+}-derived oxyhydroxides. Environmental Science and Technology, 17, 709–713.

Dzombak, D.A. and Morel, F.M. (1990) Surface Complexation Modeling, p. 393. Wiley, New York.

Emerson, S. and Widmer, G. (1978) Early diagenesis in anaerobic lake sediments-II. Thermodynamic and kinetic factors controlling the formation of Fe phosphate. Geochimica et Cosmochimica Acta, 42, 1307–1316.

Fey, M.V. and LeRoux, J. (1977) Properties and quantitive estimation of

poorly crystalline components in sesquioxidic soil clays. Clays and Clay Minerals, 25, 285–294.

Fredrickson, J.K. and Gorby, Y.A. (1996) Environmental processes mediated by Fe-reducing bacteria. Current Opinions in Biotechnology, 7, 287–294.

Fredrickson, J.K., McKinley, J.P., Bjornstad, B.N., Long, P.E., Ringelberg, D.B., White, D.C., Krumholz, L.R., Suflita, J.M., Colwell, F.S., Lehman, R.M., and Phelps, T.J. (1997) Pore-size constraints on the activity and survival of subsurface bacteria in a late Cretaceous shale-sandstone sequence, Northwestern, New Mexico. Geomicrobiology Journal, 14, 183–202.

Fredrickson, J.K., Zachara, J.M., Kennedy, D.W., Dong, H., Onslott, T.C., Hinman, N.W., and Li, S. (1998) Biogenic Fe mineralization accompanying the dissimilatory reduction of hydrous ferric oxide by a groundwater bacterium. Geochima et Cosmochimica Acta (in press).

Geelhoed, J.S., Hiemstra, T., and Van Riemsdijk, W.H. (1997) Phosphate and sulfate adsorption on goethite: Single anion and competitive adsorption. Geochimica et Cosmochimica Acta, 61, 2389–2396.

Girvin, D.C, Gassman, P.L., and Bolton, H. Jr. (1996) Adsorption of nitrilotriacetate (NTA), Co, and CoNTA by gibbote. Clays and Clay Minerals, 44, 757–768.

Jeanroy, E., Rajot, J.L, Pillon, P., and Herbillon, A.J. (1991) Differential dissolution of hematitie and geothite in dithionite and its implications in soil yellowing. Geoderma, 50, 79–94.

Kandori, K., Kawashima, Y., and Isikawa, T. (1991) Characterization of monodispersed hematite particles by gas adsorption and Fourier transform infra-red spectroscopy. Journal of chemistry Society Faraday Trans. I., 87, 2241–2246.

Kostka, J.E. and Nealson, K.H. (1995) Dissolution and reduction of magnetite by bacteria. Environmental Science and Technology, 29, 2535–2540.

Kung, K.-H. and McBride, M.B. (1988) Electron transfer processes between hydroquinone and Fe oxides. Clays and Clay Minerals, 36, 303–309.

LaKind, J.S. and Stone, A.T. (1989) Reductive dissolution of goethite by phenolic reductants. Geochimica et Cosmochimica Acta, 53, 961–971.

Lindsay, W.L. (1979) Chemical Equilibria in Soils, p. 449. Wiley-Interscience, New York.

Lovley, D.R. and Phillips, E.J.P. (1986) Availability of ferric Fe for microbial reduction in bottom sediments of the freshwater tidal Potomac River. Applied and Environmental Microbiology, 52, 751–757.

———(1987) Rapid assay for microbially reducible ferric Fe in aquatic sediments. Applied and Environmental Microbiology, 53, 1536–1540.

———(1988) Novel mode of microbial energy metabolism: organic carbon oxidation coupled to dissimilatory reduction of Fe or manganese. Applied and Environmental Microbiology, 54, 1472–1480.

Lovley, D.R., Chapelle, F.H., and Phillips, E.J.P. (1990) Fe^{3+}-reducing bacteria in deeply buried sediments of the Atlantic Coastal Plain. Geology, 16, 954–957.

Lovley, D.R., Phillips, E.J.P., and Lonergan, D.J. (1991) Enzymatic versus nonenzymatic mechanisms for Fe^{3+} reduction in aquatic sediments. Environmental Science and Technology, 25, 1062–1067.

Lovley, D.R., Coates, J.D., Blunt-Harris, E.L., Phillips, E.J.P., and Woodward, J.C. (1996) Humic substances as electron acceptors for microbial respiration. Nature, 382, 445–448.

Lovley, D.R. and Woodward, J.C. (1996) Mechanisms for chelator stimulation of microbial Fe^{3+}-oxide reduction. Chemical Geology, 132, 19–24.

Mehra, O.P. and Jackson, M.L. (1960) Fe oxide removal from soils and clays by a dithionite-citrate system buffered with sodium bi-carbonate. Clays and Clay Minerals, 7, 317–327.

Mortimer, R.J.G. and Coleman, M.L. (1997) Microbial influence on the isotopic composition of diagenetic siderite. Geochimica et Cosmochimica Acta, 61, 1705–1711.

Mortimer, R.J.G., Coleman, M.L., and Rae, J.E. (1997) Effect of bacteria on the elemental composition of early diagenetic siderite: implications for palaeoenvironmental interpretations. Sedimentology, 44, 759–765.

Myers, C.R. and Myers, J. (1997) Outer membrane cytochromes of *Shewanella putrefaciens* MR-1: spectral analysis, and purification of the 83-kDa *c*-type cytochrome. Biochimica et Biophysica Acta, 1326, 307–318.

Myers, C.R. and Nealson, K.H. (1988) Bacterial manganese reduction and growth with manganese oxide as the sole electron acceptor. Science, 240, 1319–1321.

Naono, H. and Fegiwara, R. (1980) Micropore formation due to thermal decomposition of acicular microcrystals of α-FeOOH. Journal Colloid Interface Science, 73, 406–415.

Naono, H., Nakai, K., Sueyoshi, T., and Yagi, H. (1987) Porous texture in hematite derived from goethite: mechanism of thermal decomposition of goethite. Journal Collid Interface Science, 120, 439–450.

Nilsson, N., Lovgren, L., and Sjoberg, S. (1992) Phosphate complexation at the surface of goethite. Chemical Speciation and Bioavailability, 4, 121–130.

Norrish, K. and Taylor, R.M. (1961) The isomorphous replacement of Fe by aluminum in soil goethites. Journal of Soil Science, 12, 294–306.

Olsen, S.R. and Sommers, L.E. (1982) Phosphorous. In A.L. Page, R.H. Miller, and D.R. Keeney, Eds., Methods of Soil Analysis, Part 2. Chemical and Microbiological Properties. American Society of Agronomy, 403–430.

Peterson, M.L., Brown, G.E. Jr., and Parks, G.A. (1996) Direct XAFS evidence for heterogeneous redox reaction at the aqueous chromium/magnetite interface. Colloids and Surfaces, 107, 77–88.

Phillips, E.J.P., Lovley, D.R., and Roden, E.E. (1993) Composition of nonmicrobially reducible Fe^{3+} in aquatic sediments. Applied and Environmental Microbiology, 59, 2727–2729.

Postma, D. (1981) Formation of siderite and vivianite and the pore-water composition of a recent bog sediment in Denmark. Chemical Geology, 31, 225–244.

Pye, K., Dickson, J.A.D., Schiavon, N., Coleman, M.L., and Cox, M. (1990) Formation of siderite-Mg-calcite-Fe sulphide concretions in intertidal marsh and sandflat sediments, north Norfolk, England. Sedimentology, 37, 325–343.

Roden, E.E. and Zachara, J.M. (1996) Microbial reduction of crystalline Fe^{3+} oxides: influence of oxide surface area and potential for cell growth. Environmental Science and Technology, 30, 1618–1628.

Schwertmann, U. (1964) The differentiation of Fe oxides in soil by extraction with ammonium oxalate solution. Z. Pflanzenernaehr. Dueng. Bodenk., 105, 194–202.

———(1984) The influence of aluminum on Fe oxides IX. Dissolution of Al-goethites in 6 *M* HCl. Clays and Clay Minerals, 19, 9–19.

———(1991) Solubility and dissolution of Fe oxides. Plant and Soil, 130, 1–25.

Schwertmann, U. and Cornell, R.M. (1991) Fe Oxides in the Laboratory: Preparation and Characterization. VCH Publishers, Weinheim, Germany.

Schwertmann, U., Cambier, P., and Murad, E. (1985) Properties of goethite of varying crystallinity. Clays and Clay Minerals, 33, 369–378.

Smith, R.A. and Martell, A.E. (1997). NIST Critically Selected Stability Constants of Metal Complexes Database. Version 3.0. User's Guide and Database Software. NIST Standard Reference Database no. 46. U.S. Department of Commerce, Gaithersburg, Maryland.

Stanjek, H. and Weidler, P.G. (1992) The effect of dry heating on the chemistry, surface area, and oxalate solubility of synthetic 2-line and 6-line ferrihydrites. Clay Minerals, 27, 397–412.

Stevenson, F.J. (1985) Geochimistry of Soil Humic Substances. In Aiken, G.R., McKnight, D.M., Wershaw, R.L., and MacCarthy, P., Eds., Humic Substances in Soil Sediment and Water, p. 13–52. Wiley, New York.

Stone, A.T. and Morgan, J.J. (1984) Reduction and dissolution of manganese(III) and manganese(IV) oxides by organics. 1. Reaction with quinone. Environmental Science and Technology, 18, 450–456.

Stone, A.T. and Ulrich, H.J. (1989) Kinetics and reaction stoichiometry in the reductive dissolution of manganese(IV) dioxide and Co(III) oxide by hydroquinone. Journal of Colloid and Interface Science, 132, 509–515.

Suess, E. (1979) Mineral phases formed in anoxic sediments by microbial decomposition of organic matter. Geochimica et Cosmochimica Acta, 43, 339–352.

Thorn, K.A., Arterbwin, J.B., and Mikita, M.A. (1992) ^{15}N and ^{13}C NMR

investigation of hydroxylamine-derivatized humic substances. Environmental Science and Technology, 28, 107–115.

Torrent, J., Barron, V., and Schwertmann, U. (1990) Phosphate adsorption and desorption by goethites differing in crystal morphology. Soil Science Society America Journal, 54, 1007–1012.

Torrent, J., Schwertmann, U., and Barron, V. (1992) Fast and slow phosphate sorption by goethite-rich natural materials. Clays and Clay Minerals, 40, 14–21.

Torrent, J., Schwertmann, U., and Barron, V. (1987) The reductive dissolution of synthetic goethite and hematite in dithionite. Clays and Clay Minerals, 22, 329–337.

Urrutia, M.M., Roden, E.E., Fredrickson, J.K., and Zachara, J.M. (1998) Microbial and surface chemistry controls on reduction of synthetic Fe^{3+}-oxide minerals by the dissimilatory Fe-reducing bacterium *Shewanella alga*. Geomicrobiology (in press).

Wagman, D.D., Evans, W.H., Parker, V.B., Shumm, R.H., Halow, I., Bailey, S.M., Churney, K.L., and Nuttall, R.L. (1982) The NBS tables of chemical thermodynamic properties. Selected values for inorganic and C1 and C2 organic substances in SI units. Journal of Physical Chemical Reference Data, 11, 1–392.

Weidler, P.G. (1995) Oberflachen synthetischer Eisenoxide. Dissertation, Tch University Munchen., 108.

Zachara, J.M., Smith, S.C., and Kuzel, L.S. (1995) Adsorption and dissociation of Co-EDTA complexes in Fe oxide-containing subsurface sands. Geochimica et Cosmochimica Acta, 59, 4825–4844.

Manuscript received April 30, 1998
Manuscript accepted August 20, 1998
Paper handled by Jillian F. Banfield